



LAWRENCE
LIVERMORE
NATIONAL
LABORATORY

Determining the average prompt-fission-neutron multiplicity for $^{239}\text{Pu}(n,f)$ via a $^{240}\text{Pu}(a,a')f$ surrogate reaction

B. S. Alan, J. T. Burke, O. A. Akindele, R. J. Casperson, R. O. Hughes, J. D. Koglin, K. Kolos, E. B. Norman, S. Ota, A. Saastamoinen

May 1, 2019

Physical Review C

Disclaimer

This document was prepared as an account of work sponsored by an agency of the United States government. Neither the United States government nor Lawrence Livermore National Security, LLC, nor any of their employees makes any warranty, expressed or implied, or assumes any legal liability or responsibility for the accuracy, completeness, or usefulness of any information, apparatus, product, or process disclosed, or represents that its use would not infringe privately owned rights. Reference herein to any specific commercial product, process, or service by trade name, trademark, manufacturer, or otherwise does not necessarily constitute or imply its endorsement, recommendation, or favoring by the United States government or Lawrence Livermore National Security, LLC. The views and opinions of authors expressed herein do not necessarily state or reflect those of the United States government or Lawrence Livermore National Security, LLC, and shall not be used for advertising or product endorsement purposes.

Determining the average prompt-fission-neutron multiplicity for $^{239}\text{Pu}(n,f)$ via a $^{240}\text{Pu}(\alpha,\alpha'f)$ surrogate reaction

B. S. Wang,^{1,*} J. T. Burke,¹ O. A. Akindele,^{1,2} R. J. Casperson,¹ R. O. Hughes,¹
J. D. Koglin,¹ K. Kolos,¹ E. B. Norman,^{2,1} S. Ota,³ and A. Saastamoinen³

¹*Lawrence Livermore National Laboratory, Livermore, California 94550, USA*

²*Department of Nuclear Engineering, University of California, Berkeley, California 94720, USA*

³*Cyclotron Institute, Texas A&M University, College Station, Texas 77840, USA*

(Dated: September 16, 2019)

The average prompt-fission-neutron multiplicity $\bar{\nu}$ is of significance in the areas of nuclear theory, nuclear nonproliferation, and nuclear energy. In this work, the surrogate-reaction method has been used for the first time to indirectly determine $\bar{\nu}$ for $^{239}\text{Pu}(n,f)$ via $^{240}\text{Pu}(\alpha,\alpha'f)$ reactions. A ^{240}Pu target was bombarded with a beam of 53.9-MeV α particles. Scattered α particles, fission products, and neutrons were measured with the NeutronSTARS detector array. Values of $\bar{\nu}$ were obtained for a continuous range of equivalent incident neutron energies between 0.25–26.25 MeV, and the results agree well with direct neutron measurements.

I. INTRODUCTION

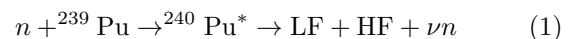
The average prompt-fission-neutron multiplicity $\bar{\nu}$ following (n,f) reactions is important to both basic and applied physics. In nuclear theory, measurements of $\bar{\nu}$ can be used to validate fission models and provide constraints on the fission process itself [1]. In the area of international safeguards and verification, nuclear materials are assayed with passive neutron-multiplicity counting, and here, $\bar{\nu}$ is needed to determine the amount of neutron-induced fission (or self-multiplication) in the sample [2, 3]. For proposed nuclear reactor concepts, such as accelerator-driven systems (ADS) and those based on the thorium-uranium cycle, there is interest in the $\bar{\nu}$ values for short-lived actinides, as the dependence of $\bar{\nu}$ on the incident neutron energy is important for determining the criticality, safety, and lifetime of these reactors [4–6]. In addition, $\bar{\nu}$ for short-lived actinides is also relevant to transmutation of radioactive waste with ADS [4–6].

Directly measuring $\bar{\nu}$ presents a number of experimental challenges, including producing high-flux neutron beams and addressing beam-related backgrounds. For short-lived actinides, $\bar{\nu}$ data are particularly sparse due to the fact that target fabrication and high target activity are also issues. These challenges can be bypassed with the surrogate-reaction method [7], an indirect measurement technique that has typically been used to determine the cross sections of reactions that proceed through a highly excited, statistically equilibrated compound nuclear state. In a surrogate experiment, the desired compound nucleus (CN) is produced using an alternative (“surrogate”) reaction with a more experimentally accessible or preferable combination of projectile and target nucleus. The surrogate method has been demonstrated to work

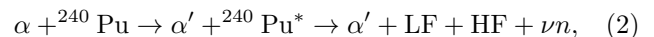
well for determining (n,f) reaction cross sections of various actinides [8–13]; the values obtained are within ~ 5 –20% of direct neutron measurements. The present work extends the applicability of this technique to determining $\bar{\nu}$. Benchmarking has been performed by using the surrogate reactions $^{240}\text{Pu}(\alpha,\alpha'f)$ and $^{242}\text{Pu}(\alpha,\alpha'f)$ to obtain $\bar{\nu}$ as a function of incident neutron energy for the reactions $^{239}\text{Pu}(n,f)$ and $^{241}\text{Pu}(n,f)$, respectively, for which direct-measurement data are available. The results for $^{239}\text{Pu}(n,f)$ are discussed in this paper, while those for $^{241}\text{Pu}(n,f)$ can be found in Ref. [14].

II. SURROGATE-REACTION TECHNIQUE

In the present work, the compound nucleus ^{240}Pu in the desired reaction



is produced via the surrogate reaction



where LF and HF are the light and heavy fission fragments, respectively, and ν is the prompt-fission-neutron multiplicity. Assuming a statistically equilibrated CN, where the decay is independent of the method of formation [15], the (n,f) cross section for an incident neutron energy E_n is given by the following Hauser-Feshbach [16–18] formula:

$$\sigma_{n,f}(E_n) = \sum_{J,\pi} \sigma_n^{CN}(E_{\text{ex}}, J, \pi) G_f^{CN}(E_{\text{ex}}, J, \pi), \quad (3)$$

where $\sigma_n^{CN}(E_{\text{ex}}, J, \pi)$ is the cross section for forming a CN with excitation energy E_{ex} , angular momentum J ,

* alan2@llnl.gov

69 and parity π , and $G_f^{CN}(E_{\text{ex}}, J, \pi)$ is the probability that
 70 the CN will fission. In the Weisskopf-Ewing limit of
 71 Hauser-Feshbach theory, where the decay of the CN is
 72 independent of J and π , Eq. 3 reduces to

$$\sigma_{n,f}(E_n) = \sigma_n^{CN}(E_{\text{ex}})G_f^{CN}(E_{\text{ex}}). \quad (4)$$

73 Analogously, the $(\alpha, \alpha'f)$ cross section for an incident α -
 74 particle energy E_α is given by

$$\sigma_{\alpha,\alpha'f}(E_\alpha) = \sigma_{\alpha,\alpha'}^{CN}(E_{\text{ex}})G_f^{CN}(E_{\text{ex}}). \quad (5)$$

75 In Eq. 4 and 5, $\sigma_n^{CN}(E_{\text{ex}})$ and $\sigma_{\alpha,\alpha'}^{CN}(E_{\text{ex}})$ are the $J\pi$ -
 76 independent CN-formation cross sections and $G_f^{CN}(E_{\text{ex}})$
 77 is the $J\pi$ -independent fission probability of the CN.
 78 If the Weisskopf-Ewing approximation applies, then
 79 (n,f) and $(\alpha,\alpha'f)$ reactions that generate the same CN
 80 with excitation energy E_{ex} will have identical values
 81 of $G_f^{CN}(E_{\text{ex}})$ and yield the same $\bar{\nu}$. The validity of
 82 this assumption is tested by comparing the $\bar{\nu}$ values
 83 obtained with the surrogate reaction $^{240}\text{Pu}(\alpha,\alpha'f)$ to
 84 those determined from direct $^{239}\text{Pu}(n,f)$ measurements.

85 III. EXPERIMENT

86 The experiment was performed in Cave 4 of the Texas
 87 A&M University Cyclotron Institute [19]. A ^{240}Pu target
 88 was loaded onto a target wheel [20] located at the center
 89 of the NeutronSTARS array [21] and bombarded with a
 90 100-pA beam of 53.9-MeV alpha particles from the K150
 91 Cyclotron; 4.75 days' worth of data was collected.

92 A. Targets

93 The ^{240}Pu target was 99.995%-pure; it was fabricated
 94 by first epoxying a $100\text{-}\mu\text{g}/\text{cm}^2$ -thick natural-carbon
 95 foil to an aluminum frame, and then electroplating
 96 plutonium onto the foil surface, covering a circular area
 97 1.90 cm in diameter. Properties of the target are given
 98 in Table I.

99 The following calibration targets were included in
 100 the experiment: a ^{208}Pb foil to determine the beam
 101 energy; a natural-carbon foil, Mylar ($(\text{C}_{10}\text{H}_8\text{O}_4)_n$) foil,
 102 and empty aluminum frame to assess backgrounds due
 103 to α interactions with carbon, oxygen and aluminum in
 104 the ^{240}Pu target. Two phosphor targets were also used
 105 for beam alignment and observing the beam-spot size.

106 B. Apparatus

107 The NeutronSTARS array is shown in Fig. 1. Charged
 108 particles, including inelastically scattered α particles
 109 from $^{240}\text{Pu}(\alpha,\alpha'f)$ reactions, were detected with a silicon

TABLE I. Properties of the ^{240}Pu target used in the
 experiment. In addition to ^{240}Pu , a small amount of ^{238}Pu
 was also present.

Property	^{240}Pu	^{238}Pu
Activity (μCi)	67.374(334)	0.250(3)
Weight Percent (%)	99.995(718)	0.00493(6)
Thickness ($\mu\text{g}/\text{cm}^2$)	104.078(528)	0.00513(6)

110 telescope located 19 mm downstream from the target
 111 and consisting of two Micron S2-type annular silicon
 112 detectors (a $152\text{-}\mu\text{m}$ -thick ΔE detector and a $994\text{-}\mu\text{m}$ -
 113 thick E detector) that were separated by 4 mm. The
 114 energy loss in the two detectors was used for particle
 115 identification. A $4.44\text{-mg}/\text{cm}^2$ -thick aluminum-foil shield
 116 was placed between the target and the telescope to
 117 prevent fission fragments and δ electrons produced in the
 118 target from damaging the ΔE detector and degrading
 119 detector performance. Fission fragments were detected
 120 with a third $146\text{-}\mu\text{m}$ -thick Micron S2 silicon detector
 121 located 19 mm upstream from the target. The silicon
 122 detectors are segmented into 48 0.5-mm-wide rings on
 123 one side and 16 22.5° -wide sectors on the other. For
 124 this experiment, pairs of adjacent rings and sectors were
 125 bussed together to form 24 1-mm-wide rings and 8 45° -
 126 wide sectors. The silicon detectors are also coated with
 127 $27\text{-}\mu\text{g}/\text{cm}^2$ aluminum contacts on the ring side and 500-
 128 $\mu\text{g}/\text{cm}^2$ gold contacts on the sector side. The gold
 129 can significantly straggle the fission fragments, making
 130 energy separation between scattered α particles and
 131 fission fragments difficult. To minimize straggling, the
 132 fission detector was installed with the ring side facing
 133 downstream and the ^{240}Pu target was mounted with the
 134 electroplated surface facing upstream.

135 The target wheel and silicon detectors were mounted
 136 inside a vacuum chamber, which was surrounded by
 137 a neutron detector (referred to as "NeutronBall")
 138 consisting of a tank filled with 3.5 tons of liquid
 139 scintillator. The tank is segmented into six regions: four
 140 identical quadrants that make up the central cylinder and
 141 two endcaps. Twenty photomultiplier tubes (PMTs),
 142 three on each quadrant and four on each endcap, are
 143 used to measure scintillation light. At the time of
 144 the measurement, the central cylinder was filled with
 145 fresh EJ-335 liquid scintillator doped with 0.25-wt%
 146 of natural gadolinium [22]; however the two endcaps
 147 contained degraded liquid scintillator with poor optical
 148 transmission. Therefore, in the present work, only events
 149 detected by the twelve PMTs on the central cylinder were
 150 included in the data analysis.

151 C. Detector calibrations

152 For the ΔE and E detectors, the response of each ring
 153 and sector was calibrated with a ^{226}Ra α point source
 154 that provided the following α lines: 4784, 5304, 5489,

155 6002, and 7687 keV [23]. At 7687 keV, the resulting 1σ
 156 energy resolutions for the ΔE detector and E detector
 157 were approximately 40 keV and 24 keV, respectively. The
 158 fission detector was calibrated with a ^{252}Cf spontaneous
 159 fission source. The light and heavy fission-product mass
 160 peaks were used to gain match the response of the rings.
 161 For NeutronBall, ^{60}Co and ^{228}Th γ -ray point sources
 162 provided calibration points at 1253 keV (the average
 163 energy of the 1173-keV and 1332-keV γ rays from ^{60}Co)
 164 and 2615 keV (from ^{208}Tl in the ^{228}Th decay chain)
 165 [23]. Another calibration point was provided by the 4440-
 166 keV γ rays [23] that were emitted following inelastic α
 167 scattering with the natural-carbon target that promoted
 168 ^{12}C to its first excited state. The energy resolution of the
 169 liquid scintillator at energy E (in MeV) was $\sigma(E)/E =$
 170 $25\%/\sqrt{E}$ [21].

171 The efficiency for detecting a single neutron with the
 172 central cylinder of NeutronBall was determined to be
 173 $0.504(5)$ and was measured by placing a ^{252}Cf fission
 174 source at the target position. More details will be given
 175 in Sec. IV C.

176 D. α -particle beam

177 The α -particle beam-spot size was approximately
 178 3 mm in diameter and was observed with an in-vacuum
 179 camera that imaged the phosphor targets. The exact
 180 beam energy provided by the K150 Cyclotron was
 181 determined from data collected for the ^{208}Pb target.
 182 Scattering of α particles to discrete states in ^{208}Pb
 183 was used as an *in situ* calibration. The beam energy was
 184 determined to be 53.9(1) MeV. This value allowed the
 185 excitation energy of the ^{208}Pb nucleus to be properly
 186 reconstructed after taking into account the energy
 187 deposition in the ΔE - E telescope, the energy loss in
 188 dead layers (i.e., the target, the aluminum-foil shield,
 189 and the gold and aluminum contacts on the surfaces of
 190 the silicon detectors), and the recoil energy of the ^{208}Pb
 191 nucleus. The uncertainty in the beam energy was taken
 192 to be the 1σ width of the α peak corresponding to elastic
 193 scattering.

194 IV. ANALYSIS AND RESULTS

195 A $^{240}\text{Pu}(\alpha, \alpha' f)$ interaction was indicated by a
 196 coincidence between an α particle hitting the silicon
 197 telescope and a fission fragment hitting the fission
 198 detector. For a ^{240}Pu CN with excitation energy E_{ex} ,
 199 corresponding to an equivalent incident neutron energy
 200 E_n , the average prompt-fission-neutron multiplicity was
 201 determined from

$$\bar{\nu}(E_n) = \frac{N_n(E_n)}{N_{\alpha-f}(E_n)\epsilon_n}, \quad (6)$$

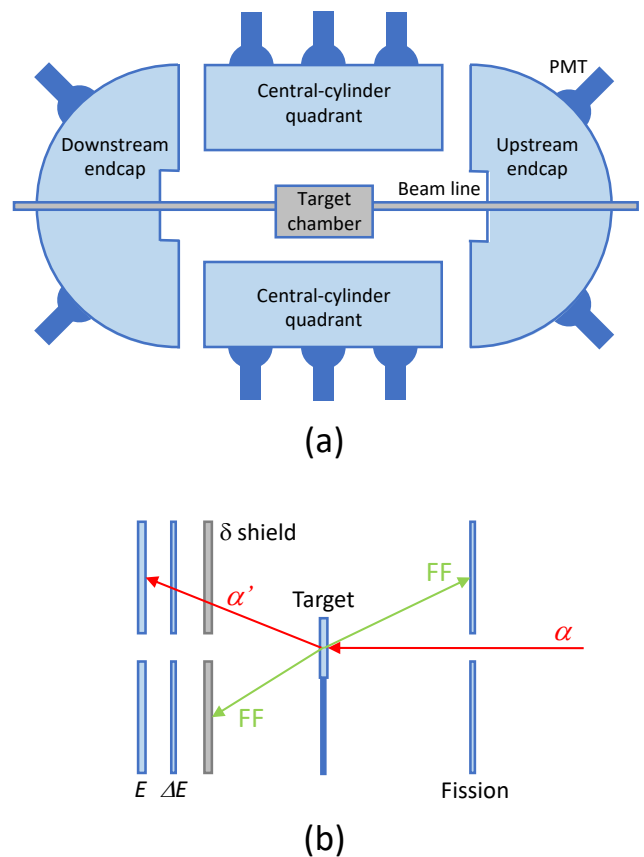


FIG. 1. (Color online) Cross-sectional views of (a) the NeutronSTARS detector array and (b) the inside of the target chamber (not to-scale); the α -particle beam travels from right to left. NeutronSTARS consists of a target chamber that sits at the center of a neutron detector. The latter is a large tank of gadolinium-doped liquid scintillator segmented into six regions: four identical quadrants that make up the central cylinder and two endcaps. Three PMTs are attached to each quadrant and four are attached to each endcap. The target chamber contains a target wheel, a ΔE - E telescope to measure scattered α particles, a fission detector to measure fission fragments (FF), and a δ shield to prevent fission fragments and δ electrons from hitting the ΔE detector.

202 where $N_{\alpha-f}(E_n)$ is the number of measured
 203 $^{240}\text{Pu}(\alpha, \alpha' f)$ α -fission coincidences at E_n , $N_n(E_n)$
 204 is the number of detected prompt fission neutrons
 205 associated with these coincidences, and ϵ_n is the single-
 206 neutron detection efficiency for the central cylinder of
 207 NeutronBall. The analysis performed to obtain the
 208 quantities in Eq. 6 is discussed in this section, and the
 209 resulting $\bar{\nu}(E_n)$ distribution is given.

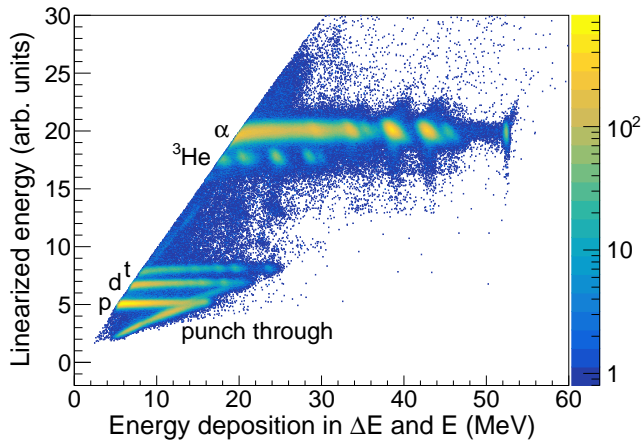


FIG. 2. (Color online) Particle-identification plot for 53.9-MeV α particles incident on ^{240}Pu . The linearized energy versus the total energy deposited in both the ΔE and E detectors is shown for events hitting a chosen ring in the ΔE detector. Bands corresponding to protons (p), deuterons (d), tritons (t), ^3He , and α particles (α) are indicated. The diagonal streaks are due to high-energy charged particles that “punch through” the E detector and therefore do not deposit all of their energy in the telescope.

A. Particle identification and event selection

1. Charged particles

For events in the silicon telescope, the energies deposited in the ΔE and E detectors ($E_{\Delta E}$ and E_E , respectively) were used for particle identification (PID). Protons, deuterons, tritons, ^3He , and α particles were distinguished by plotting the “linearized energy” E_{lin} [24] versus the total energy deposition in both the ΔE and E detectors, where

$$E_{\text{lin}} = [(E_{\Delta E} + E_E)^{1.75} - E_E^{1.75}]^{1/1.75}. \quad (7)$$

Alpha-particle events were isolated by generating a PID plot for each ΔE -detector ring (e.g., Fig. 2) and gating on the region above ^3He (E_{lin} approximately between 16.5–24).

2. Fission

Fig. 3 shows the gain-matched spectrum measured by a single ring on the fission detector for α particles incident on the ^{240}Pu target. A double hump is present at higher energies due to heavy and light fission fragments hitting the detector. The large peak at lower energies is primarily due to light ions from ^{240}Pu α decay and α -particle interactions with carbon and oxygen in the ^{240}Pu target, which was confirmed by analysis of the data collected for the natural-carbon and Mylar targets.

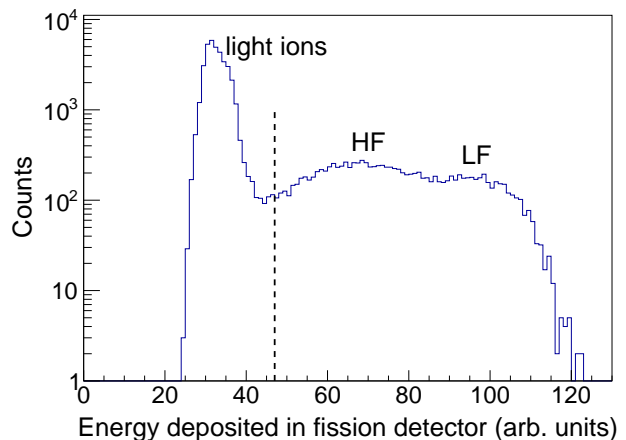


FIG. 3. Gain-matched spectrum measured by a single ring on the fission detector for 53.9-MeV α particles incident on ^{240}Pu . Peaks corresponding to heavy fission fragments (HF), light fission fragments (LF), and light ions are labeled. A vertical line is drawn at the energy cut used to separate fission fragments and light ions.

For each ring, fission events were selected and light-ion events removed by cutting above an energy deposition of 47 (arb. units).

3. $^{240}\text{Pu}(\alpha, \alpha' f)$ events

In Fig. 4, the time difference between coincident ΔE - E α -particle and fission-detector events is plotted; the energy deposited in the fission detector is given along the y axis. A horizontal line is drawn at the energy cut-off used to isolate fission fragments from light ions. Coincidences above the cut-off with a time difference between -35 ns and 86 ns (“prompt” region) were tagged as $^{240}\text{Pu}(\alpha, \alpha' f)$ events. The small bursts of events present every 121 ns in Fig. 4 coincide with the K150 cyclotron frequency and are due to random coincidences such as an α particle hitting the ΔE - E telescope and a fission fragment from a $^{240}\text{Pu}(\alpha, f)$ reaction in the target hitting the fission detector.

4. Neutrons

PMT signals that arrived within a coincidence window of 200 ns were assumed to come from a single event in NeutronBall, e.g., a neutron capture on gadolinium, or an interaction of a room-background γ ray. These signals were first gain matched, as described in Ref. [21], then summed together to acquire the total energy deposited by the event. Only events with energy greater than 2 MeV were included in the data analysis to exclude most of the contribution from backgrounds and electronic noise.

For the tagged $^{240}\text{Pu}(\alpha, \alpha' f)$ events, a timing gate was opened 50 μs before and closed 500 μs after the

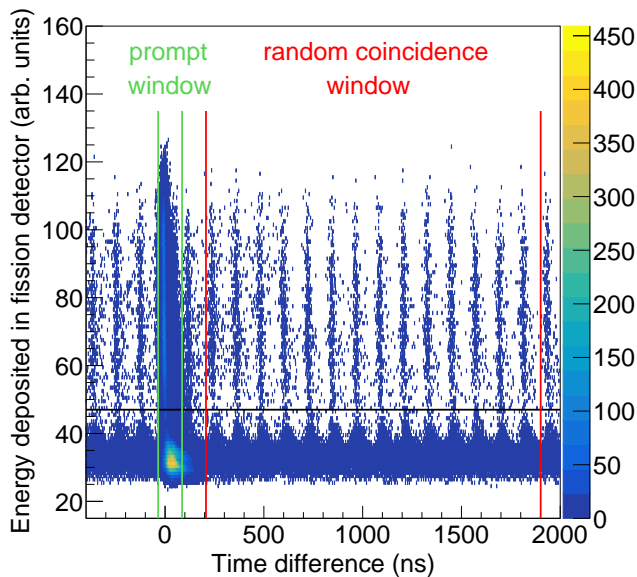


FIG. 4. (Color online) Coincidences between an α particle hitting the ΔE - E telescope and an event in the fission detector. The energy deposited in the fission detector is plotted versus the fission-detector event time minus the α -particle event time. A horizontal line is drawn at the energy cut-off used to isolate fission fragments from light ions. Vertical lines indicate the gates used in the data analysis to identify and characterize prompt α -fission coincidences (-35 ns to 86 ns) and random-coincidences (207 to 1901 ns).

262 α -fission coincidence. The time difference between a
 263 NeutronBall event occurring within this gate and the α -
 264 fission coincidence was plotted (Fig. 5). The sharp peak
 265 around $0 \mu\text{s}$ in Fig. 5 is from the flash of prompt γ rays
 266 following fission and from proton recoils generated during
 267 thermalization of the neutron in the liquid scintillator.
 268 The broad peak above $0 \mu\text{s}$ is attributed to prompt fission
 269 neutrons; its width is determined by the moderation time
 270 of the neutrons in the scintillator. Both features lie on
 271 top of a flat background due to random coincidences.

B. Equivalent neutron energy

273 The excitation energy E_{ex} of ^{240}Pu following inelastic
 274 α -particle scattering was determined from the beam
 275 energy E_{α} , the scattered- α -particle energy $E_{\alpha'}$, and the
 276 ^{240}Pu recoil energy E_r :

$$E_{\text{ex}} = E_{\alpha} - E_{\alpha'} - E_r. \quad (8)$$

277 The value of $E_{\alpha'}$ was the total energy deposited in the
 278 ΔE - E telescope corrected for energy losses in the target,
 279 the δ shield, and the inert gold and aluminum contacts
 280 on the surfaces of the silicon detectors. The equivalent
 281 incident neutron energy E_n was then determined from

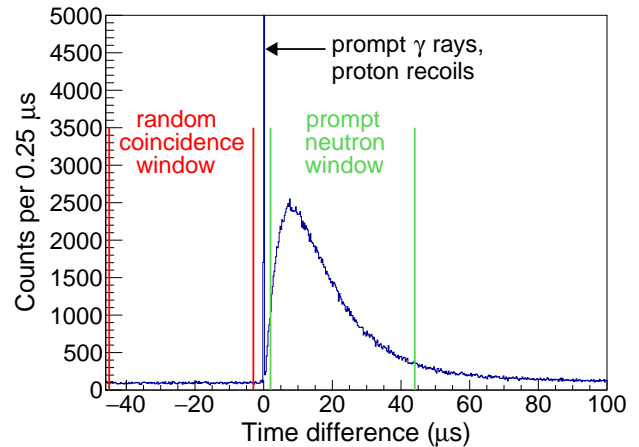


FIG. 5. (Color online) Time difference between an event in NeutronBall and an α -fission coincidence tagged as a $^{240}\text{Pu}(\alpha, \alpha' f)$ event. The peak due to prompt fission γ rays and proton recoils is indicated. The time windows used in the analysis to gate on prompt fission neutrons (2 to $44 \mu\text{s}$) and random coincidences (-45 to $-3 \mu\text{s}$) are also shown.

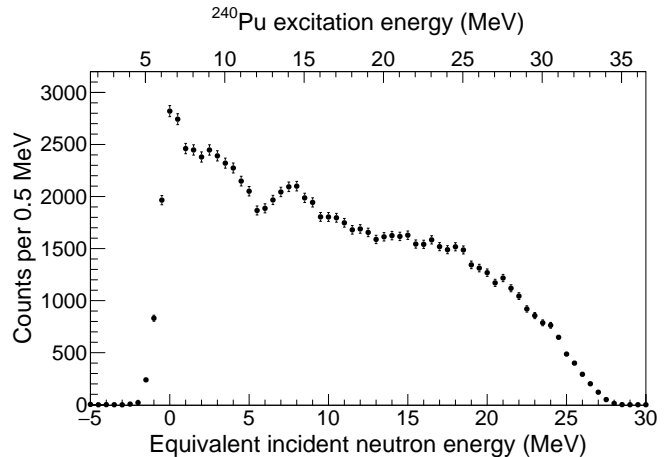


FIG. 6. The distribution of equivalent incident neutron energies (and corresponding ^{240}Pu excitation energies) for $^{240}\text{Pu}(\alpha, \alpha' f)$ events; 0.5 -MeV-wide energy bins are used.

$$E_n = \frac{m_t + m_n}{m_t} (E_{\text{ex}} - S_n), \quad (9)$$

282 where m_t is the mass of ^{239}Pu , m_n is the neutron
 283 mass, and S_n is the neutron separation energy for ^{240}Pu .
 284 Fig. 6 shows the E_n distribution for $^{240}\text{Pu}(\alpha, \alpha' f)$ events.
 285 The corresponding ^{240}Pu excitation energy is also given.
 286 Fission of ^{240}Pu starts to occur at $E_n = -1.61$ MeV
 287 (4.9 -MeV ^{240}Pu excitation energy) [25]. The feature
 288 at $E_n \sim 5.5$ MeV is due to ^{240}Pu second-chance fission
 289 [26, 27], and above $E_n \sim 18.5$ MeV, the number of events
 290 tapers off quickly due to the α -Pu Coulomb barrier.

291 C. Average prompt-fission-neutron multiplicity

292 The average prompt-fission-neutron multiplicity was
 293 obtained with Eq. 6 for equivalent incident neutron
 294 energies ranging between 0.25 and 26.25 MeV. The
 295 quantity $N_{\alpha-f}(E_n)$ in Eq. 6 is the number of α -fission
 296 coincidences in the (121-ns-wide) prompt region of Fig. 4,
 297 corrected for the contribution from random coincidences.
 298 This contribution was determined by taking the sum of α -
 299 fission coincidences in the region 207–1901 ns and scaling
 300 down to a 121-ns-wide time window.

301 The number of neutrons $N_n(E_n)$ was obtained by
 302 taking the difference between the total counts in the
 303 time regions 2 to 44 μ s and -45 to -3 μ s in Fig. 5.
 304 The contribution from random α -fission coincidences
 305 was determined from the time-difference spectrum for
 306 NeutronBall events associated with the 207–1901-ns
 307 region in Fig. 4 (scaled down to correspond to a 121-
 308 ns-wide α -fission time window).

309 A single-neutron detection efficiency of $\epsilon_n = 0.504(5)$
 310 was obtained by first recording the time-difference
 311 between ^{252}Cf fission events in the fission detector and
 312 events in NeutronBall. The total number of prompt
 313 neutrons measured was then determined and divided by
 314 the number of fission events and $\bar{\nu}$ for ^{252}Cf (i.e., 3.757)
 315 [28, 29].

316 The $\bar{\nu}(E_n)$ distribution obtained is given in Fig. 7.
 317 Each $\bar{\nu}$ value and its uncertainty is also provided in
 318 Table II; the uncertainty is dominated by the statistical
 319 uncertainties in the number of α -fission coincidences and
 320 the number of detected neutrons. Fig. 7 also shows that
 321 the results of the present work are consistent with direct
 322 neutron measurements for $^{239}\text{Pu}(n,f)$ [30–35], providing
 323 validation that the surrogate-reaction method can be
 324 used to determine $\bar{\nu}$ for actinides.

325 V. SUMMARY AND CONCLUSIONS

326 $^{240}\text{Pu}(\alpha,\alpha'f)$ was used as a surrogate reaction
 327 to determine the $^{239}\text{Pu}(n,f)$ prompt-fission-neutron
 328 multiplicity as a function of incident neutron energy from
 329 0.25–26.25 MeV. This is the first time $\bar{\nu}$ for $^{239}\text{Pu}(n,f)$
 330 has been obtained continuously over this neutron energy
 331 range in a single measurement. The results of the present
 332 work are in good agreement with those from direct
 333 neutron measurements [30–35]. Similar conclusions
 334 were drawn in Ref. [14], where the surrogate reaction
 335 $^{242}\text{Pu}(\alpha,\alpha'f)$ was used to determine $\bar{\nu}$ for $^{241}\text{Pu}(n,f)$.
 336 The success of these two experiments opens the door to
 337 using surrogate reactions to obtain $\bar{\nu}(E_n)$ for a whole host
 338 of short-lived actinides that are currently inaccessible via
 339 direct methods.

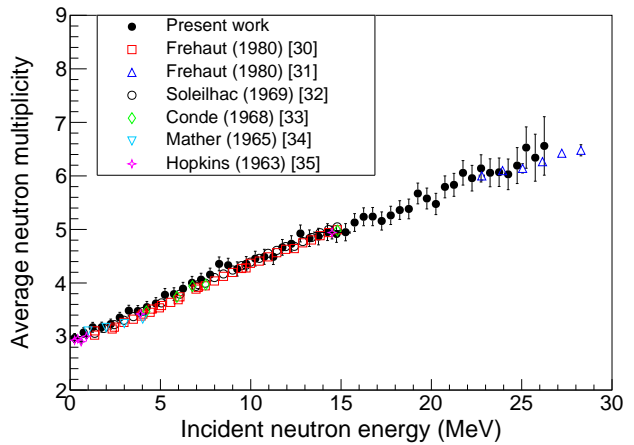


FIG. 7. (Color online) The average prompt-fission-neutron multiplicity $\bar{\nu}$ as a function of incident neutron energy for $^{239}\text{Pu}(n,f)$. In the present work, $\bar{\nu}$ has been determined continuously from 0.25–26.25 MeV in 0.5-MeV-wide intervals. The results are compared with direct neutron measurements found in literature [30–35]. In the present work the uncertainties are primarily due to counting statistics; for the literature values, most of the uncertainties are smaller than the data markers.

TABLE II. Equivalent incident neutron energies E_n and corresponding $\bar{\nu}$ values from the present work.

E_n (MeV)	$\bar{\nu}$	E_n (MeV)	$\bar{\nu}$
0.25	2.97(8)	13.75	4.87(15)
0.75	3.08(9)	14.25	4.95(16)
1.25	3.17(9)	14.75	4.92(16)
1.75	3.17(9)	15.25	4.95(16)
2.25	3.23(9)	15.75	5.13(17)
2.75	3.35(10)	16.25	5.24(17)
3.25	3.48(10)	16.75	5.24(17)
3.75	3.48(10)	17.25	5.16(17)
4.25	3.55(11)	17.75	5.26(17)
4.75	3.62(11)	18.25	5.36(17)
5.25	3.78(12)	18.75	5.38(18)
5.75	3.79(12)	19.25	5.67(19)
6.25	3.89(12)	19.75	5.58(19)
6.75	4.00(12)	20.25	5.48(20)
7.25	4.06(12)	20.75	5.80(20)
7.75	4.16(12)	21.25	5.83(21)
8.25	4.36(13)	21.75	6.06(23)
8.75	4.33(13)	22.25	5.96(24)
9.25	4.26(13)	22.75	6.14(25)
9.75	4.36(13)	23.25	6.06(26)
10.25	4.46(14)	23.75	6.07(27)
10.75	4.49(14)	24.25	6.03(29)
11.25	4.49(14)	24.75	6.19(34)
11.75	4.67(15)	25.25	6.53(39)
12.25	4.73(15)	25.75	6.34(44)
12.75	4.93(16)	26.25	6.56(55)
13.25	4.84(15)		

VI. ACKNOWLEDGMENTS

We thank the staff of the Texas A&M Cyclotron Institute for facilitating operations and facilities needed to perform this measurement. This work was performed under the auspices of the U.S. Department

of Energy National Nuclear Security Administration by Lawrence Livermore National Laboratory under Contract No. DE-AC52-07NA27344, under Award No. DE-NA0000979, and through the Nuclear Science and Security Consortium under Award No. DE-NA-0003180.

- [1] V. M. Maslov, Y. V. Porodzinskij, M. Baba, A. Hasegawa, N. V. Kornilov, A. B. Kagalenko, and N. A. Tetereva, *Phys. Rev. C* **69**, 034607 (2004).
- [2] N. Ensslin, W. C. Harker, M. S. Krick, D. G. Langner, M. M. Pickrell, and J. E. Stewart, Los Alamos National Laboratory, LA-13422-M (1998).
- [3] T. H. Shin, M. Y. Hua, M. J. Marcath, D. L. Chichester, I. Pázsit, A. D. Fulvio, S. D. Clarke, and S. A. Pozzi, *Nucl. Sci. Eng.* **188**, 246 (2017).
- [4] T. Ethvignot, M. Devlin, H. Duarte, T. Granier, R. C. Haight, B. Morillon, R. O. Nelson, J. M. O'Donnell, and D. Rochman, *Phys. Rev. Lett.* **94**, 052701 (2005).
- [5] D. Kerdraon, A. Billebaud, R. Brissot, B. Carlucci, S. David, D. Heuer, C. Le Brun, E. Liatard, J.-M. Loiseaux, O. Méplan, E. Merle, H. Nifenecker, and D. Verrier, *Prog. Nucl. Energy* **42**, 11 (2003).
- [6] H. Nifenecker, S. David, J. Loiseaux, and O. Meplan, *Nucl. Instrum. Methods Phys. Res. A* **463**, 428 (2001).
- [7] J. E. Escher, J. T. Burke, F. S. Dietrich, N. D. Scielzo, I. J. Thompson, and W. Younes, *Rev. Mod. Phys.* **84**, 353 (2012).
- [8] M. Petit, M. Aiche, G. Barreau, S. Boyer, N. Carjan, S. Czajkowski, D. Dassié, C. Grosjean, A. Guiral, B. Haas, D. Karamanis, S. Misicu, C. Rizea, F. Saintamon, S. Andriamonje, E. Bouchez, F. Gunsing, A. Hurstel, Y. Lecoz, R. Lucas, C. Theisen, A. Billebaud, L. Perrot, and E. Bauge, *Nucl. Phys. A* **735**, 345 (2004).
- [9] C. Plettner, H. Ai, C. W. Beausang, L. A. Bernstein, L. Ahle, H. Amro, M. Babilon, J. T. Burke, J. A. Caggiano, R. F. Casten, J. A. Church, J. R. Cooper, B. Crider, G. Gürdal, A. Heinz, E. A. McCutchan, K. Moody, J. A. Punyon, J. Qian, J. J. Ressler, A. Schiller, E. Williams, and W. Younes, *Phys. Rev. C* **71**, 051602(R) (2005).
- [10] J. T. Burke, L. A. Bernstein, J. Escher, L. Ahle, J. A. Church, F. S. Dietrich, K. J. Moody, E. B. Norman, L. Phair, P. Fallon, R. M. Clark, M. A. Deleplanque, M. Descovich, M. Cromaz, I. Y. Lee, A. O. Macchiavelli, M. A. McMahan, L. G. Moretto, E. Rodriguez-Vieitez, F. S. Stephens, H. Ai, C. Plettner, C. Beausang, and B. Crider, *Phys. Rev. C* **73**, 054604 (2006).
- [11] J. E. Escher and F. S. Dietrich, *Phys. Rev. C* **74**, 054601 (2006).
- [12] S. R. Leshner, J. T. Burke, L. A. Bernstein, H. Ai, C. W. Beausang, D. L. Bleuel, R. M. Clark, F. S. Dietrich, J. E. Escher, P. Fallon, J. Gibelin, B. L. Goldblum, I. Y. Lee, A. O. Macchiavelli, M. A. McMahan, K. J. Moody, E. B. Norman, L. Phair, E. Rodriguez-Vieitez, N. D. Scielzo, and M. Wiedeking, *Phys. Rev. C* **79**, 044609 (2009).
- [13] J. J. Ressler, J. T. Burke, J. E. Escher, C. T. Angell, M. S. Basunia, C. W. Beausang, L. A. Bernstein, D. L. Bleuel, R. J. Casperson, B. L. Goldblum, J. Gostic, R. Hatarik, R. Henderson, R. O. Hughes, J. Munson, L. W. Phair, T. J. Ross, N. D. Scielzo, E. Swanberg, I. J. Thompson, and M. Wiedeking, *Phys. Rev. C* **83**, 054610 (2011).
- [14] O. A. Akindele, B. S. Alan, J. T. Burke, R. J. Casperson, R. O. Hughes, J. D. Koglin, K. Kolos, E. B. Norman, S. Ota, and A. Saastamoinen, *Phys. Rev. C* **99**, 054601 (2019).
- [15] N. Bohr, *Nature* **137**, 344 (1936).
- [16] W. Hauser and H. Feshbach, *Phys. Rev.* **87**, 366 (1952).
- [17] P. Fröbrich and R. Lipperheide, *Theory of Nuclear Reactions* (Clarendon Press, 1996).
- [18] I. J. Thompson and F. M. Nunes, *Nuclear Reactions for Astrophysics: Principles, Calculation and Applications of Low-Energy Reactions* (Cambridge University Press, 2009).
- [19] G. Tabacaru, H. Clark, J. Arje, and D. May, *AIP Conf. Proc.* **2076**, 040002 (2019).
- [20] S. R. Leshner, L. Phair, L. A. Bernstein, D. L. Bleuel, J. T. Burke, J. A. Church, P. Fallon, J. Gibelin, N. D. Scielzo, and M. Wiedeking, *Nucl. Instrum. Methods Phys. Res. A* **621**, 286 (2010).
- [21] O. A. Akindele, R. J. Casperson, B. S. Wang, J. T. Burke, R. O. Hughes, S. E. Fisher, A. Saastamoinen, and E. B. Norman, *Nucl. Instrum. Methods Phys. Res. A* **872**, 112 (2017).
- [22] "EJ-331, EJ-335 Data Sheet, Eljen Technology," https://eljentechology.com/images/products/data_sheets/EJ-331_EJ-335.pdf.
- [23] R. R. Kinsey, C. L. Dunford, J. K. Tuli, and T. W. Burrows, 9th International Symposium on Capture Gamma-Ray Spectroscopy and Related Topics, Budapest, Hungary (1996), data extracted from the NUDAT database, version 2.7.
- [24] F. S. Goulding, D. A. Landis, J. Cerny, and R. H. Pehl, *IEEE Trans. Nucl. Sci.* **11**, 388 (1964).
- [25] J. A. Northrop, R. H. Stokes, and K. Boyer, *Phys. Rev.* **115**, 1277 (1959).
- [26] J. P. Lestone and T. T. Strother, *Nucl. Data Sheets* **118**, 208 (2014).
- [27] I. Stetcu, P. Talou, and T. Kawano, *EPJ Web Conf.* **122**, 01012 (2016).
- [28] J. W. Boldeman and M. G. Hines, *Nucl. Sci. Eng.* **91**, 114 (1985).
- [29] J. Boldeman and A. Dalton, Australian Atomic Energy Commission, AAEC/E172 (1967).
- [30] J. Frehaut, G. Mosinski, and M. Soleilhac, Data retrieved from CSISRS database, file EXFOR 20490 (1980).
- [31] J. Frehaut, Data retrieved from CSISRS database, file EXFOR 21685 (1980).
- [32] M. Soleilhac, J. Frehaut, and J. Gauriau, *J. Nucl. Energy* **23**, 257 (1969).

- ⁴⁵⁵ [33] H. Condé, J. Hansén, and M. Holmberg, J. Nucl. Energy ⁴⁵⁹ [35] J. C. Hopkins and B. C. Diven, Nucl. Phys. **48**, 433
⁴⁵⁶ **22**, 53 (1968). ⁴⁶⁰ (1963).
- ⁴⁵⁷ [34] D. S. Mather, P. Fieldhouse, and A. Moat, Nucl. Phys.
⁴⁵⁸ **66**, 149 (1965).